Fracture controlled paleohydrogeology in a basement-cored, fault-related fold: Sheep Mountain Anticline, Wyoming, United States

Nicolas Beaudoin, Nicolas Bellahsen, Olivier Lacombe, Laurent Emmanuel

Geochemistry Geophysics Geosystems G3

Article
Volume 12, Number 6
24 June 2011
Q06011, doi:10.1029/2010GC003494
ISSN: 1525-2027

Published by AGU and the Geochemical Society

Fracture-controlled paleohydrogeology in a basement-cored, fault-related fold: Sheep Mountain Anticline, Wyoming, United States

Nicolas Beaudoin, Nicolas Bellahsen, Olivier Lacombe, and Laurent Emmanuel
ISTEP, UMR 7193, UPMC Université de Paris 6, CNRS, F-75005 Paris, France
(nicolas.beaudoin@upmc.fr)

[1] New geochemical and microstructural data constrain the origins and pathways of paleofluids during the growth of Sheep Mountain Anticline, Wyoming, United States. Oxygen, carbon, and strontium isotope studies were performed on prefolding and fold-related calcite veins and their sedimentary host rocks and combined to fluid inclusion microthermometry results. We show that most of the cements precipitated from Paleogene meteoric fluid. Stable isotopes and fluid inclusion homogenization temperatures further indicate that most veins were mineralized from upward moving fluids after these fluids were heated at depth (T > 110°C). This implies that fluids migrated along the basement thrust underlying the fold and/or at the base of the cover. Above the fault tip, the fluids circulated rapidly in the diffuse synfolding (and early folding) fracture network. The zone of preferential migration of the warm fluids is currently located in the backlimb of the fold, which supports some of the previously published structural interpretation of the subsurface. This study also highlights the potential of combined fracture analysis and geochemical analyses of paleofluid flows in fractures to constrain both the deformation history and the fluid flow during basement-involved shortening in Laramide-style forelands.

Components: 8000 words, 9 figures, 1 table.

Keywords: Laramide foreland; calcite veins; folding; fracture pattern; paleofluids; stable isotopes.

Index Terms: 8005 Structural Geology: Folds and folding; 8010 Structural Geology: Fractures and faults; 8045 Structural Geology: Role of fluids.

Received 3 January 2011; **Revised** 18 April 2011; **Accepted** 18 April 2011; **Published** 24 June 2011.

Beaudoin, N., N. Bellahsen, O. Lacombe, and L. Emmanuel (2011), Fracture-controlled paleohydrogeology in a basement-cored, fault-related fold: Sheep Mountain Anticline, Wyoming, United States, *Geochem. Geophys. Geosyst.*, *12*, Q06011, doi:10.1029/2010GC003494.

1. Introduction

[2] Fluid flow is a first-order feature of deformations in foreland basins. The fluids can have either basinal, meteoric or hydrothermal origin [*Marquer and Burkhard*, 1992; *Travé et al.*, 2000; *Van Geet et al.*, 2002; *Roure et al.*, 2005; *Katz et al.*, 2006; *Travé et al.*, 2007]. Their migration pathways and interactions with host rocks can be determined by paleohydrological studies of (diagenetic) cements and mineralized veins [*Dietrich et al.*, 1983; *Conti et al.*, 2001; *Lefticariu et al.*, 2005; *Katz et al.*, 2006, *Fischer et al.*, 2009]. Specific interactions between fluid flows and faults (i.e., behaving as conduits or barriers) have been the focus of most of the studies [*Dietrich et al.*, 1983; *Foreman and Dunne*, 1991; *Templeton et al.*, 1995]. They show that periods of successive closed (enhanced fluid-rock interactions) and open (reduced fluid-rock

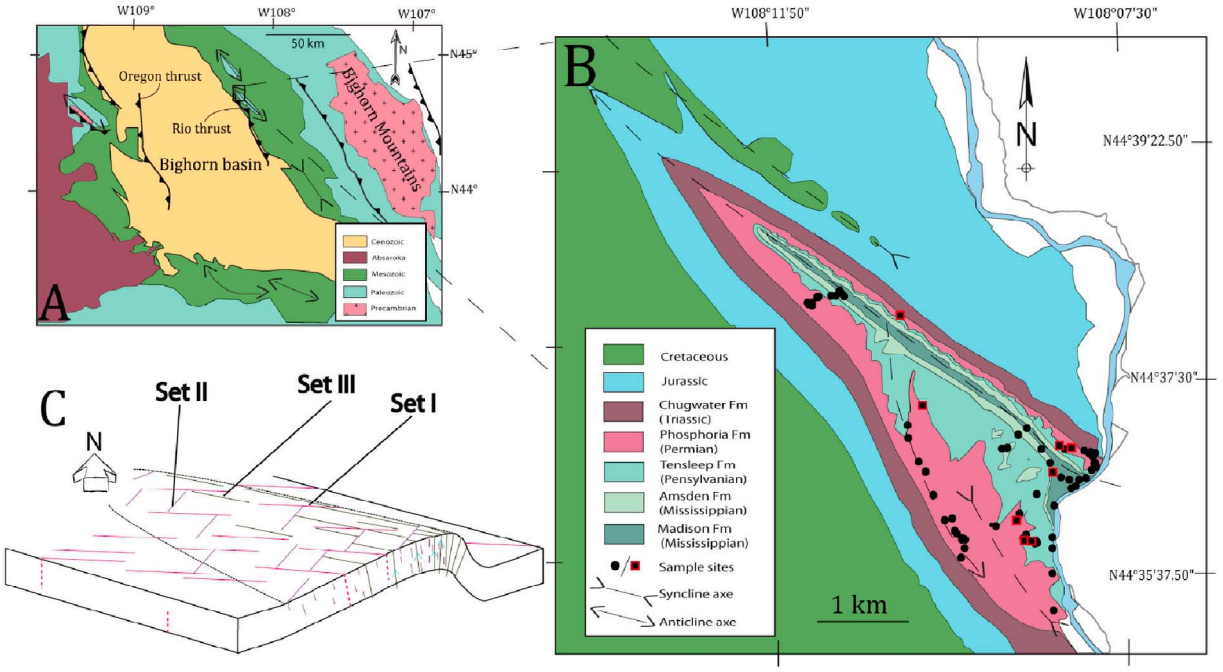

Figure 1. (a) Simplified geological and structural map of the Bighorn Basin. (b) Simplified geological map of the NW part of Sheep Mountain Anticline. Dots and squares correspond to sampling locations. (c) First-order fracture pattern in SMA after *Bellahsen et al.* [2006a].

interactions) fluid systems may be recognized during the evolution of various fault zones and have helped to constrain the timing of activation of superimposed décollement levels [*Travé et al.*, 2000] or the initiation of detachment faulting [*Templeton et al.*, 1995].

[3] However, only a few studies have dealt with fluid flows in diffuse fracture patterns in folds [*Travé et al.*, 2000; *Fischer et al.*, 2009], although the large-scale movement of fluids through rocks of relatively low matrix permeability may occur. This low permeability can be overcome by the formation and connection of (early and synfolding) fractures facilitating irregular and punctuated fluid migration events [e.g., *Lefticariu et al.*, 2005; *Fischer et al.*, 2009]. This behavior makes map-scale folds one of the most complicated hydrogeological settings, where many unanswered questions remain. Most paleohydrological studies focused on thin-skinned fold-and-thrust belts and usually describe meteoric fluids flowing within the cover through conduits like faults [*Ramsey and Onasch*, 1999; *Douglas et al.*, 2003; *Evans and Hobbs*, 2003; *Bussolotto et al.*, 2007]. Very few works aimed at studying fluid flow during basement-involved tectonics. In such settings, key questions are as follows. At which scale does fluid flow occur in such system? Do the fluids flow within the basement or in the cover only? What are the consequences of preferential fluid pathways on the geochemistry of these fluids and host rocks? What is the timing of such circulations, especially in the framework of the initiation and development of the main faults and fracture sets? Are the diffuse fracture sets efficient conduits? What is the role of fluid flows in the microstructural (and macrostructural) evolution?

[4] In this contribution, a study of the oxygen, carbon and strontium isotope composition of calcite veins and their host sedimentary rocks enables us to constrain the paleohydrological system evolution of the Sheep Mountain Anticline (SMA), a Laramide, basement-cored anticline in Wyoming, United States (Figure 1a) [*Hennier*, 1984; *Forster et al.*, 1996; *Stanton and Erslev*, 2004; *Stone*, 2004; *Erslev*, 2005]. Even if the geometry of the underlying thrust is still debated [*Hennier and Spang*, 1983; *Forster et al.*, 1996, *Stanton and Erslev*, 2004; *Stone*, 2004, *Fiore Allwardt et al.*, 2007, *Amrouch et al.*, 2010a], the structure and timing of the fracture network in this fold is well constrained [*Harris et al.*, 1960; *Johnson et al.*, 1965; *Bellahsen et al.*, 2006a, 2006b; *Amrouch et al.*, 2010a; *Savage et al.*, 2010], and allows us to accurately place our geochemical study into a reliable spatiotemporal context related to the evolution of the fold. Our primary goal is to constrain the paleofluid system at

the fold scale, and to relate the evolution of this system to the evolution of the fold. To this purpose, we performed observations under cathodoluminescence microscopy and geochemical isotopic studies (C, O, Sr) on well-recognized prefolding and synfolding calcite veins in order to reconstruct syntectonic fluid flow. An additional microthermometric fluid inclusion study was carried out in order to complement an earlier diagenetic study of the Madison Formation [*Katz et al.*, 2006] by extending it to all formations that crop out at SMA.

2. Geological and Microstructural Settings

[5] Sheep Mountain Anticline (SMA) is a Laramide fold located along the northeastern edge of the Bighorn Basin, Wyoming, United States (Figure 1a). SMA is a 28 km long asymmetrical fold striking NW-SE, with a wavelength of 4 km and amplitude of 1000 m. The backlimb dips 30° toward the Southwest and the forelimb 70° toward the Northeast. The sedimentary cover comprises the Mississipian limestones/dolostones of the Madison Formation, the Mississipian shales and sandstones of the Amsden Formation, the Pennsylvanian sandstones of the Tensleep Formations, and the Permian limestones of the Phosphoria Formation. These strata form a competent core in the 3000 m thick sedimentary cover, principally made of shales (above and below the above mentioned formations) [*Hennier*, 1984]. SMA is classically interpreted as a basement-cored fold related to a southwest dipping back thrust soled on the SW verging Rio thrust [*Stanton and Erslev*, 2004]. On the southwest, in the backlimb, a rabbit ear structure striking 170°E, oblique to the fold trend, is connected to the main fold (Figure 1b).

[6] *Bellahsen et al.* [2006a] investigated the fracture pattern at SMA and defined three main fracture sets related to distinct stages of fold history (Figure 1c). Set I comprises bed-perpendicular joints and veins striking 110°–130°E after unfolding (tentatively related to a Sevier phase by *Amrouch et al.* [2010a]) opened in mode I (i.e., pure tension). These fractures often present tail cracks at their end, consistent with their later left-lateral reactivation during the Laramide event (NE-SW shortening). Set II is composed of 045°E bed-perpendicular joints and veins with mode I opening mainly observed in the hinge and the backlimb, related to Laramide Layer-Parallel Shortening (LPS). These fractures affect all formations. According to *Bellahsen et al.* [2006b], their spatial pattern suggests a stress perturbation above the basement fault tip causing a stress shadow that inhibited development of set II joints in sedimentary layers of the future forelimb. Set III comprises 135°E, curvature-related mode I joints and veins, parallel to the fold axis and mainly present at and near the fold hinge. The asymmetry of SMA, highlighted at the macroscopic scale by the spatial distribution of set II fractures, is also clearly marked in the strain pattern at the microscopic scale [*Amrouch et al.*, 2010b].

3. Analytical Methods

3.1. Sampling

[7] We collected 125 samples in various structural positions (backlimb, hinge, forelimb), lithologies (sandstones and limestones), formations (Madison, Amsden, Tensleep, Phosphoria), and fracture sets (sets I, II, III). Sampling was concentrated along two cross sections and along the rabbit ear structure (Figure 1b). Each studied oriented sample consists of one or more veins with a width between 0.3 and 1.5 cm, and an attached piece of host rock.

3.2. X-Ray Diffraction and Cathodoluminescence Microscopy

[8] Representative host rocks and cements were analyzed by X-ray powder diffraction on a SIEMENS D501 X-ray diffractometer. In order to investigate the diagenetic state of both veins and host rocks, preliminary petrographic observations were done on polished thin sections of 30 μm thickness under an optical microscope. The diagenetic state, the microstructural characteristics and the crosscutting relationships of both host rocks and veins were determined under cathodoluminescence microscopy using a cathodoluminescence Cathodyne Opea device with a cold cathode system. Operating conditions were in the range of 200–400 μA and 13–18 kV gun current and at a constant 60 milliTorr vacuum.

3.3. Oxygen and Carbon Stable Isotope Analysis

[9] The $\delta^{13}C$ and $\delta^{18}O$ analyses were performed using an automated preparation device coupled to an Isoprime gas ratio mass spectrometer in order to constrain the geochemical signature of calcite cements of veins, the origin of fluids from which those cements precipitate and so the paleofluid system evolution through space and time. Veins were hand drilled or micromilled to avoid mixture with host rocks. Samples were placed in glass vials and reacted with dehydrated phosphoric acid under

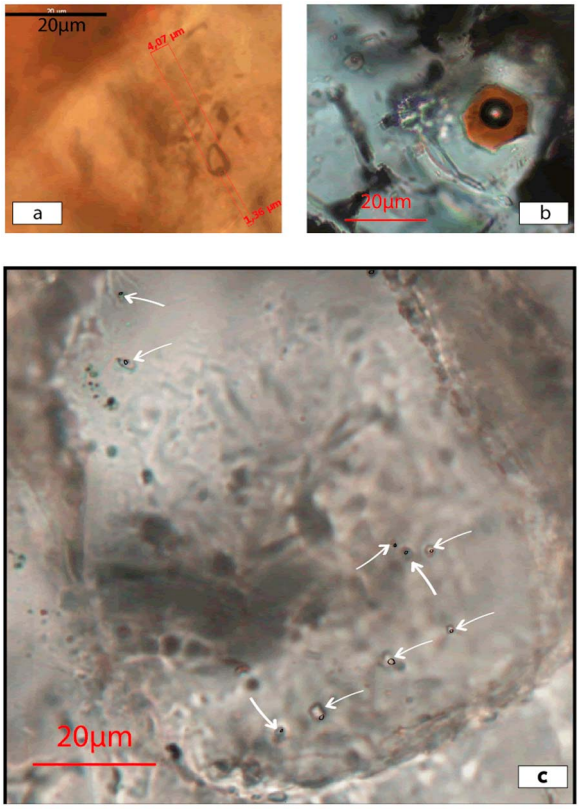

Figure 2. Photomicrographs showing examples of the kind of inclusions we studied in samples. (a) A two-phase aqueous inclusion hosted in the Phosphoria Formation, sample 09P. (b) An assemblage of two-phase oil-bearing inclusion hosted in the Phosphoria Formation, sample 13P; note that the bubble is big and the high vapor-liquid ratio suggest that the internal volume was not conserved during the crystal history. These kinds of fluid inclusions were not taken into account for our interpretations. (c) An assemblage of primary two-phase aqueous inclusion hosted in the Tensleep Formation, sample 47T; note that the vapor-liquid ratio seems to be low and constant in this assemblage. All photos were taken at 25°C.

vacuum at 90°C, necessitating a correction for dolomite samples according to *Rosenbaum and Sheppard* [1986]. Values are reported in permil (‰) relative to the Vienna Peedee belemnite (VPDB/PDB) for carbon and for oxygen with an accuracy of 0.05‰ and 0.1‰, respectively (Table S1 with detailed results is provided in the auxiliary material).[1]

3.4. Strontium Isotope Analysis

[10] We used $^{87}Sr/^{86}Sr$ isotopes on nine representative samples to define the origin and migration pathways of paleofluids (reported as open squares in Figure 1a). The analyses were performed at the Geochronology and Isotopic Geochemistry Laboratory in the "Universidad Complutense de Madrid." The analyzed cements were chosen according to the hosting fracture set and to their $\delta^{13}C$ and $\delta^{18}O$ isotopic signature. Previously weighted samples of calcite in Teflon® vials were dissolved in 3 ml of pure 2.5M hydrochloric acid, over a period of 2 h at room temperature. After this time, samples were centrifuged at 4000 r.p.m. for 10 min. Sr was separated from other elements using cation exchange chromatography with Dowex 50W-X12 resin. Sr samples were collected in clean vials and evaporated at 80°C. Dry Sr samples were loaded along with 1 μl of phosphoric acid (1M) over a single tantalum filament and were introduced into the Micromass VG Sector-54 Thermal Ionization Mass Spectrometer (TIMS) and analyzed using a dynamic multicollection method (five Faraday detectors) with 150 scans. Strontium results were corrected for ^{87}Rb interferences. The $^{87}Sr/^{86}Sr$ ratios were normalized using as reference the radiogenic stable ratio ($^{88}Sr/^{86}Sr$: 0.1194). This normalization corrects the mass fractionation in the sample through the load and the total analysis time. SRM 987 was chosen as isotopic standard of Sr to analyze at the same time with samples. Each sample was analyzed eight times with an analytical error of the laboratory in the $^{87}Sr/^{86}Sr$ ratio of 0.01% (average values are reported in Table S1).

3.5. Microthermometric Study of Fluid Inclusions

[11] To complement and to check a previous fluid inclusion study performed at SMA on the Madison Formation [*Katz et al.*, 2006], 100 μm doubly polished thick sections were prepared and analyzed on a Linkam Pr 600 microthermometric stage. For this study, sampling was focused on the Tensleep sandstones and Phosphoria limestones wherein 17 nondeformed two-phase primary fluid inclusions were identified. Inclusions seemingly have low vapor-liquid ratios (Figure 2a), which are constant in the same assemblage (Figure 2c). The diagenetic state of the crystals hosting the inclusions was checked using classical microscopy (on the studied thick sections) and by cathodoluminescence microscopy (on a mirror thin section). Samples were heated at a rate of 15°C per minute until the vapor bubble decreased in size; heat rate was slowed at less than 1°C per minute in order to determine the homogenization temperature of the fluid inclusion. All measurements are reproducible with an accuracy

[1] Auxiliary materials are available in the HTML. doi:10.1029/2010GC003494.

Table 1. Results of Microthermometric Fluid Inclusion Study[a]

Sample	Set	Formation	Location	Number of Inclusions Measured	Homogeneization Temperature (°C)	Ice Melting Temperature (°C)	$\delta^{18}O$ (‰PDB)	Note
18	3	Tensleep	Backlimb	4	113 to 124	UM	−20.82	
V1-2	2	Phosphoria	Forelimb	3	107 to 135	−10.4 to −1.2	−22.81	
47	2	Tensleep	Hinge	2	115 to 116	UM	−22.935	
13	2	Phosphoria	Backlimb	2	71.5 to 72.2	UM	−17.89	
13	2	Phosphoria	Backlimb	5	98.6 to 202	UM	−17.89	Oil-bearing fluid inclusion
45		Phosphoria	Backlimb	6	105.3 to 110.5	−1.5 to −1		
SM 1.95 m[b]	ND	Madison	ND	39	120 to 140	>0	−22.7	

[a]All temperatures are given ±0.5°C. ND, not determined; UM, unable to measure.
[b]These values are related to cemented veins in the Madison Formation at SMA [*Katz et al.*, 2006].

of ±0.5°C. Then, two-phase inclusions were frozen until the vapor bubble disappeared and only ice remained, and they were reheated in order to determine the ice melting temperature, relative to the fluid salinity. Despite analytical care, some decrepitation of the fluid inclusions happened after the first heating phase, preventing the determination of the ice melting temperature of some samples. Our data are presented in Table 1 together with those of *Katz et al.* [2006].

4. Results

4.1. Mineralogy and Petrography

[12] In most samples the mineralized veins are filled with pure calcite while the host rocks comprise dolomite or sandstone. Under cathodoluminescence, host rocks display a red dolomite-related luminescence, whereas veins display an orange calcite-related luminescence. Three kinds of luminescence texture are displayed by the veins, each of which we interpret as representing unique precipitation conditions: (1) an orange calcite-related luminescence in the whole vein with a homogeneous texture, which is evidence that precipitation occurred in constant oxidation reduction conditions and at near constant rates, probably fast (Figure 3a), (2) a luminescence highlighting the mineral growth with concentric zonations from bright to dull orange and without irregularities on grain boundaries, which indicates that the cement precipitated during a single event of fluid flow either under different oxidation reduction conditions, or at different precipitation rates (Figure 3b), (3) two phases of calcite filling in the same vein (Figure 3c). In this last setting, there is a phase with concentric zonations of luminescence from bright to dull orange starting from the edge of the vein and a second filling phase which have dull orange calcite-related homogeneous luminescence at the center of the vein. In between, irregular grain margins (labeled d in Figure 3c) suggest there was a period of chemical dissolution of the first cement, supporting the interpretation that the cements have precipitated during two different migration events [*Cazenave et al.*, 2003; *Chapoulie et al.*, 2005] with calcite precipitating slower in the first event and faster in the second one. Although the first two described luminescence textures are observed in all fracture sets, the third texture is only observed in some of set II veins.

4.2. Oxygen and Carbon Stable Isotopes

[13] A total of 145 isotopic analyses were performed on samples from 80 veins and 65 pieces of host rock. The $\delta^{13}C$ and $\delta^{18}O$ values of cements are plotted according to the fracture set together with their host rock $\delta^{13}C$ and $\delta^{18}O$ values (Figure 4a). Veins and host rocks exhibit a wide range of isotopic signature for both oxygen and carbon ($-23‰ < \delta^{18}O < -1‰$; $-25‰ < \delta^{13}C < +4‰$). Host rocks show a narrower range of $\delta^{18}O$ (−9‰ to 4‰) and of $\delta^{13}C$ (−9‰ to 6‰) values. Calcite veins display a variable range of isotopic values depending on the fracture sets. Sevier-related reactivated veins from set I have the widest variation in oxygen values (blue circles: $-22.5‰ < \delta^{18}O < -2‰$; $-17‰ < \delta^{13}C < -2‰$). Laramide LPS-related veins (set II) have the widest variation in carbon values (red triangles: $-23‰ < \delta^{18}O < -12‰$; $-25‰ < \delta^{13}C < -0.5‰$). Synfolding set III veins are characterized by a narrower range of $\delta^{18}O$ and $\delta^{13}C$ signatures (green squares: $-23‰ < \delta^{18}O < -19‰$, $-13‰ < \delta^{13}C < -5‰$). The isotopic data from uncorrelated fracture sets show a range of $\delta^{18}O$ and $\delta^{13}C$ values similar to the range of isotopic values related to set I (black stars: $-22‰ < \delta^{18}O < -2‰$; $-24.5‰ < \delta^{13}C < -1‰$).

[14] The comparison of the isotopic signatures of veins and host rocks in the different formations

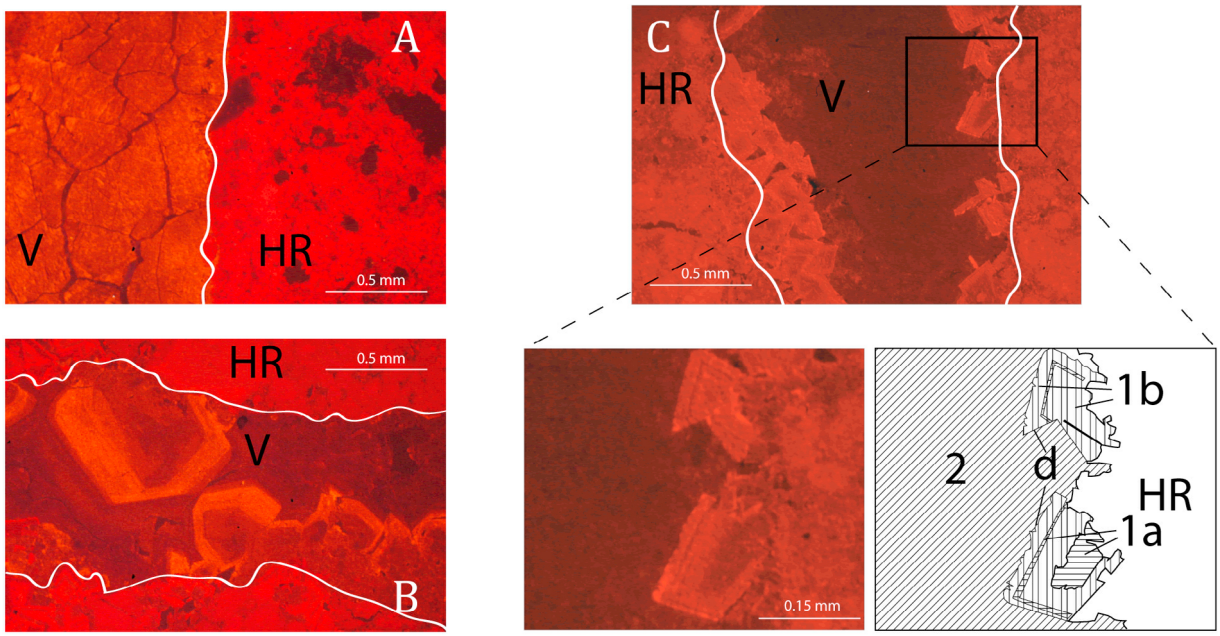

Figure 3. Cathodoluminescence observation of veins exhibiting three kinds of luminescence. White lines separate veins cement (V) from host rock cement (HR). (a) Homogeneous filling of vein by cement with calcite-related bright orange luminescence. (b) Filling of vein by cement exhibiting calcite-related bright to dull orange luminescence with concentric zonations. (c) Two phases of calcite related filling in a single vein with evidence for chemical dissolution. The different growth phases are represented on the interpretative sketch: HR, host rock; 1a, first growth phase in an environment favorable to Mn incorporation; 1b, first growth phase in an environment unfavorable to Mn incorporation; d, boundary of first growth phase solution; 2, second growth phase in an environment likely unfavorable to Mn incorporation.

(Figure 4b), irrespective of fracture orientation and timing, shows that the slopes of the trend lines illustrating the interactions between the fluids and the host rocks are different in limestone units (Madison and Phosphoria formations) and in sandstone units (Tensleep Formation). This explains that two mixing lines appear on the $\delta^{13}C$ versus $\delta^{18}O$ plot. Moreover, in the sandstone unit, there is a gap of equilibration between veins and host rocks around $\delta^{18}O = -15‰$, suggesting that equilibration is more efficient in limestones than in sandstones.

[15] Curves of $\delta^{18}O$ isovalues were drawn on a detailed map of the fold (Figure 5). The values used to define the isopleths are the less depleted $\delta^{18}O$ ratios of the Laramide related sets, respectively −19‰ for the set III and −12‰ for the set II. Isopleths were hand drawn considering all veins regardless of sets and formations. The 40 isotopic data of sets I, II and III veins were used for that construction, and only five veins did not fit. As a result, a zone of much depleted $\delta^{18}O$ ratios ($\delta^{18}O \leq -19‰$) is highlighted within the three fracture sets. Strikingly, this zone has a trend parallel to the fold hinge, but is shifted southwestward away from it regardless of lithology, especially in the northwestern part of the fold, suggesting that the corresponding fluid flow is fold related.

4.3. Strontium Isotopes

[16] The $^{87}Sr/^{86}Sr$ ratios were measured in nine vein samples in order to determine whether fluids which precipitate in Laramide-related fractures previously interacted with Rb-rich source rocks, such as granites and gneisses, during their migration. $^{87}Sr/^{86}Sr$ ratios are reported in Table S1 and have been plotted against $\delta^{18}O$ with regard to the fracture sets (Figure 5). Since Sr isotopes are not considered to have significant mass fractionation during most geological processes, including precipitation [e.g., *Faure and Powell*, 1972], the $^{87}Sr/^{86}Sr$ ratio of a vein provides a direct information about the migration pathways of the fluid. In order to consider the equilibration processes during the fluid migration, strontium isotope compositions of Mississippian seawater ($^{87}Sr/^{86}Sr$ = 0.70750–0.70850), and of Paleozoic and Jurassic sedimentary cover ($^{87}Sr/^{86}Sr$ = 0.70700–0.70900) were also reported in Figure 6. We also consider the values of Laramide arches

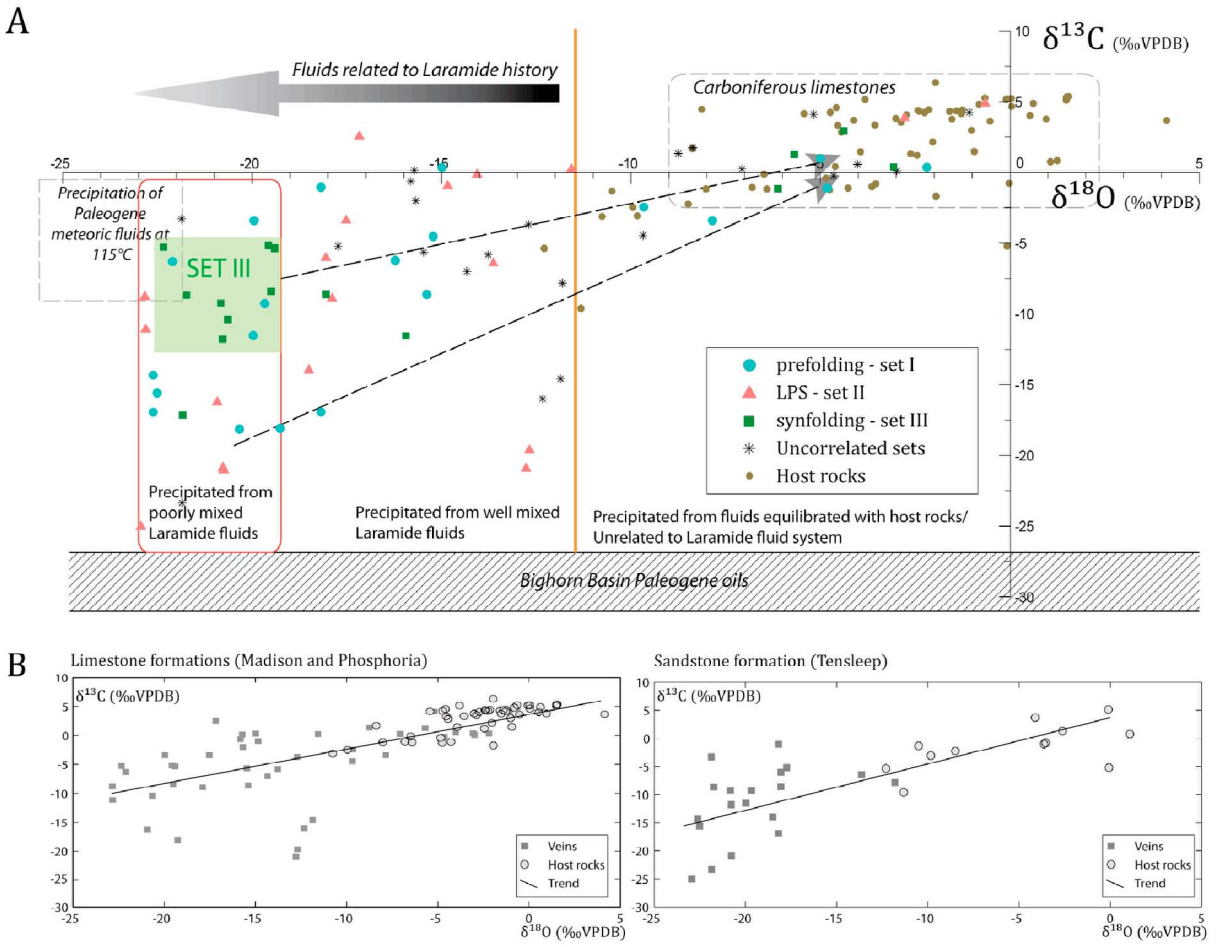

Figure 4. (a) The $\delta^{18}O$ versus $\delta^{13}C$ isotopic values of vein and host rock samples from SMA. Paleogene meteoric fluid isotopic values are shown as a dashed square and were taken from *Koch et al.* [1995] but were modified for isotopic fractionation of oxygen, which was calculated by using the precipitation equation for calcite ↔ H_2O [*Zheng*, 1999] and for isotopic fractionation of carbon, which was calculated by using the precipitation equation for calcite ↔ CO_2 [*Bottinga*, 1969]. These equations consider a closed system with temperature between 0°C and 1200°C for oxygen and between 0°C and 600°C for carbon. The Carboniferous limestone isotopic range was reported by *Katz et al.* [2006], and the Bighorn Basin hydrocarbon isotopic range was reported by *Chung et al.* [1981]. (b) The $\delta^{18}O$ versus $\delta^{13}C$ isotopic values of carbonate and sandstone formations in veins and host rocks. The trends are reported as black lines. All values are in per mil relative to Vienna Peedee belemnite (VPDB).

Precambrian basement rocks ($^{87}Sr/^{86}Sr$ = 0.73110–0.93992), which were not reported in Figure 6. Strontium isotope composition of Paleogene meteoric water ($^{87}Sr/^{86}Sr$ = 0.71205) was also added, according to an estimate from Eocene limestones of Lake Gosiute, located in the near Green River Basin [*Rhodes et al.*, 2002]. Unradiogenic vein cements appear to be related to basinal fluids, as indicated by the $\delta^{18}O$ values of these samples; they likely indicate a mix between basinal fluids and heated meteoric fluids. Thus, these Sr isotope analyses suggest that fluids involved in the system are a mix between basinal fluids and meteoric fluids. A mixing line was generated in order to quantify the mix between the two main external sources of fluids. It appears that the proportion of meteoric fluid can reach 50% in the mix with more local basinal fluids.

4.4. Microthermometric Study of Fluid Inclusions

[17] In order to complement the study of fluid inclusions carried out in the Madison Formation by *Katz et al.* [2006], we performed a microthermometric fluid inclusion study in five additional samples from the Phosphoria and Tensleep

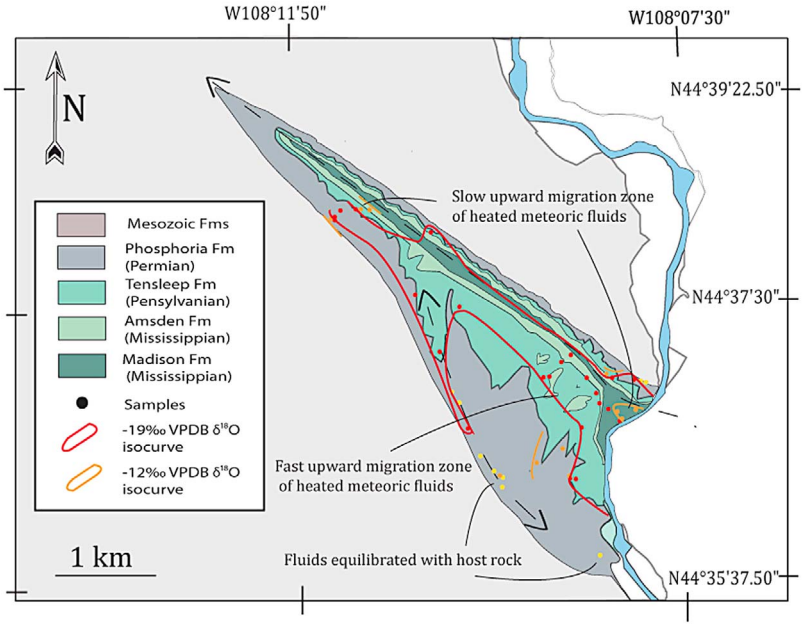

Figure 5. Plots of δ^{18}O isovalues in map view. The -19‰ PDB and −12‰ PDB isovalues range are related to the less depleted δ^{18}O ratios of the main fast upward fluid migration (i.e., set III) and of the Laramide fluid flow (i.e., set II), respectively. All isotopic values are in permil relative to VPDB.

formations (Table 1). The results show mainly hot fluids flowing in SMA (homogenization temperature T > 110°C) consistent with the previous estimates (120°C < T < 140°C) [*Katz et al.*, 2006]. These homogenization temperatures were used as estimates of the minimum filling (entrapment) temperature of fluids [*Hanor*, 1980]. Thus, the δ^{18}O values of these fluids were calculated according to the isotopic fractioning coefficients established by *Kim and O'Neil* [1997]. Homogenization temperature, calculated δ^{18}O values of the fluids and measured δ^{18}O values of cements (represented as oblique lines) are represented altogether on the same plot (Figure 7). All samples plotted are lined up on a range of δ^{18}O of fluid values between −7‰ standard mean ocean water (SMOW) and 4‰ SMOW and

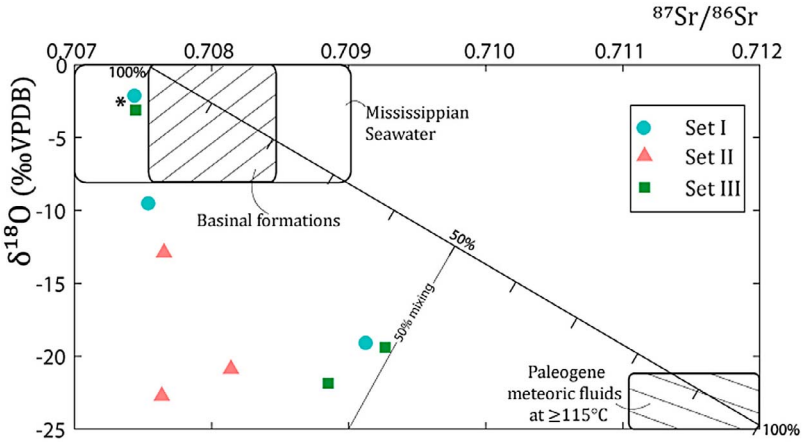

Figure 6. Strontium (^{87}Sr/^{86}Sr) and oxygen isotope (‰ PDB) crossplot of vein calcite according to the fracture set. Strontium isotope values for Mississippian seawater are from *Bruckschen et al.* [1999], whereas Paleozoic and Jurassic basinal and Paleogene meteoric values are from *Rhodes et al.* [2002]. A mixing line between Paleogene heated meteoric fluids and basinal fluids have been reported in order to quantify the degree of mixing of fluids that precipitated. Samples denoted with an asterisk are related to Laramide noncorrelated veins totally equilibrated with host rock.

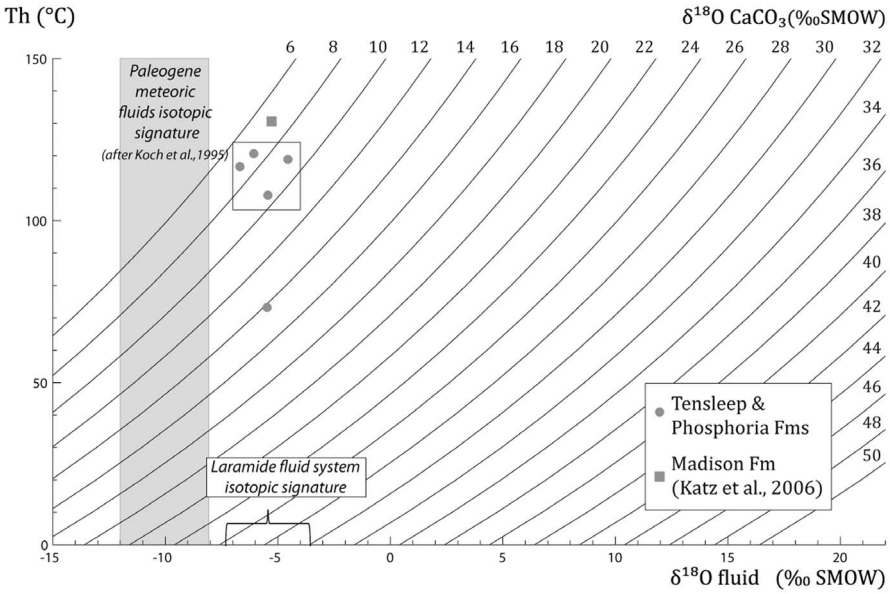

Figure 7. The δ^{18}O isotopic values of vein calcite (standard mean ocean water (SMOW), oblique lines) against δ^{18}O isotopic values (SMOW) of fluid, calculated as a function of crystallization temperature, approximated by homogenization temperatures measured by fluid inclusion microthermometry [see also *Bussolotto et al.*, 2007]. The calculations were made after the *Kim and O'Neil* [1997] precipitation fractionation equation.

two different temperatures are highlighted: most of the samples reveal fluids around 115°C and one reveals fluids at 70°C.

[18] Five oil-bearing fluid inclusions were also found in the Phosphoria Formation. However, because their appearance and their vapor-liquid ratios suggest that they were likely deformed (Figure 2b) [*Bodnar*, 2003; *Goldstein and Reynolds*, 1994], they could not be studied in term of microthermometry. Nevertheless, their occurrence is important in the determination of fluid flow in the system, because hydrocarbon migration in the eastern part of the Bighorn Basin is related to the Laramide orogeny, and it involves the Madison Formation as the source rock [*Stone*, 1967; *Chung et al.*, 1981; *Bjorøy et al.*, 1996]. Thus, oil-bearing fluid inclusions in the Phosphoria Formation veins support an upward fluid flow in the veins, an important constraint on the final fluid migration scenario.

5. Discussion

[19] We collected structural and geochemical data that constrain the fracture-controlled paleofluid system at Sheep Mountain Anticline. In sections 5.1–5.3, we describe this system by defining the degree of fluid-rock interaction, the characteristics and sources of the fluids and the fluid migration pathways. Finally, we briefly discuss the structural implications of these data.

5.1. Fluid-Rock Interactions in Fracture Sets

[20] Figures 4 and 8 show that different degrees of fluid-rock interaction occurred in vein/fracture sets. We believe this reflects different rates of fluid migration at different times in the different vein sets. The isotopic signature of all our host rocks is similar to that reported by *Katz et al.* [2006] for the Madison Limestone (Figure 4a). The δ^{18}O and δ^{13}C isotopic signatures of the fracture sets show a wide range for set I and II and a narrower one for set III (Figure 4a). Note that some isotopic values of both set I, set II and set III veins exhibit a total equilibration with respect to their host rocks (Figures 4a and 8) which is also supported by cathodoluminescence microscopy. As they witness a chemically closed system, they will not be considered as being representative of any fluid flow and will not be taken into account in the following discussion. In contrast, the narrow isotopic range of set III veins (Figure 4a, green squares), with δ^{18}O values significantly different from host rocks, suggests that fluids precipitating in these veins migrated at rates that were fast enough to maintain their high temperature and avoid efficient isotopic equilibration with host rocks. The

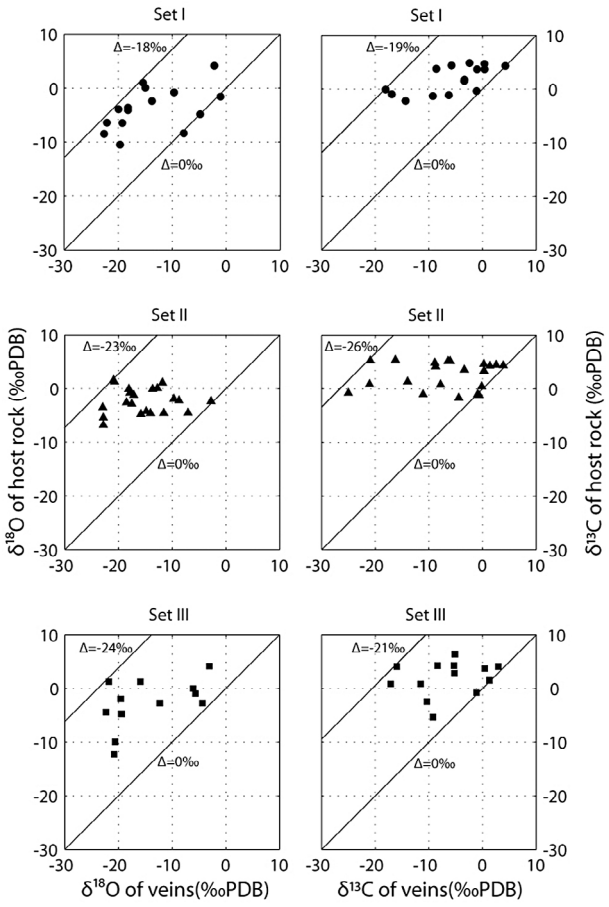

Figure 8. The δ^{18}O vein calcite versus δ^{18}O limestone host rock and δ^{13}C vein calcite versus δ^{13}C limestone host rock for each fracture set. Solid circles indicate set I veins, solid triangles indicate set II veins, and solid squares indicate set III veins. Solid lines and Δ values reported are the isotope shift (‰ PDB) related to the degree of isotopic equilibration between vein cements and host rock.

isotopic range of LPS-related set II veins (Figure 4a, red triangles and Figure 8) suggests that fluids had variable degrees of interaction with host rocks. Thus, set II fractures were probably poorly efficient conduits. Set I veins have the widest range of isotopic values (Figure 4a, blue circles and Figure 8): this suggests either a nonpermeable fracture pattern and/or a complex fluid system, which could be related to both pre-Laramide or post-Laramide evolution of the fold. Finally, the isotopic signatures of uncorrelated fractures, similar to the isotopic signatures of set I veins (Figure 4a, black stars), could also reflect a similar long and complex fluid flow history. Only set III fractures appear to have been efficient conduits for fluid flow within SMA, allowing fast migration of fluids through the cover. We hypothesize that this was related (1) to an increase of fracture density at the onset of folding, (2) to an increase of fracture connectivity (due to abutting fractures with different orientation), and (3) to the field-documented large vertical persistence of these fractures, in contrast to the mainly stratabound set II fractures (J. P. Callot, personal communication, 2009). These fast migrating, warm, unequilibrated fluids, present in nearly all set III veins, in most of set II veins and in some set I veins, therefore represent the "Laramide paleofluid system" that was present at Sheep Mountain Anticline. As suggested by *Fischer et al.* [2009] in another fold, the fluid system recorded by most of the veins is mainly related to the development of the Laramide-related fracture pattern.

5.2. Origin and Characteristics of Paleofluids Involved in the System

[21] The entire Laramide fluid system shared the same meteoric source, mixed to various degrees with basinal fluids (Figures 6 and 7). Hence, the isotope values of Paleogene meteoric water can be supposed as the fluid isotope reference, because the Laramide contractional event is mainly Paleogene in age. *Koch et al.* [1995] showed that Paleogene meteoric fluids have an isotopic signature about $-12‰ < \delta^{18}O < -8‰$ relative to SMOW and $-5‰ < \delta^{13}C < +3‰$ relative to PDB (Figure 4a, dashed square). We consider the isotopic signature of the Paleogene meteoric fluids as if they had precipitated at a temperature of 115°C as indicated by microthermometric study of fluid inclusion [*Katz et al.*, 2006; this study]. Thus, the isotopic range of cements precipitated from the Paleogene meteoric water is about $-25.9‰ < \delta^{18}O < -21.9‰$ and $-8.2‰ < \delta^{13}C < -0.2‰$ relative to PDB, values that are slightly more negative in oxygen and more positive in carbon than the range of calcite values determined for set III veins. Moreover, as shown in Figure 7, a similar shift separates the isotopic values of Paleogene meteoric fluid and the isotopic values of the fluid that is inferred to have been the source for calcite veins precipitated between 70 and 130°C. Two processes can together explain the isotopic shift observed between the Paleogene meteoric fluids and the fluids precipitated in Laramide fractures: (1) a minimal isotopic equilibration between fluids and host rocks (Figure 4b) and (2) the mix of meteoric fluids with basinal fluids (Figure 6). The wide range in δ^{13}C values of all vein cements is likely related to a local contamination with hydrocarbons [e.g., *Hathaway and Degens*, 1969; *Donovan et al.*, 1974; *Boles et al.*, 2004], and thus supports a mix with basinal fluids.

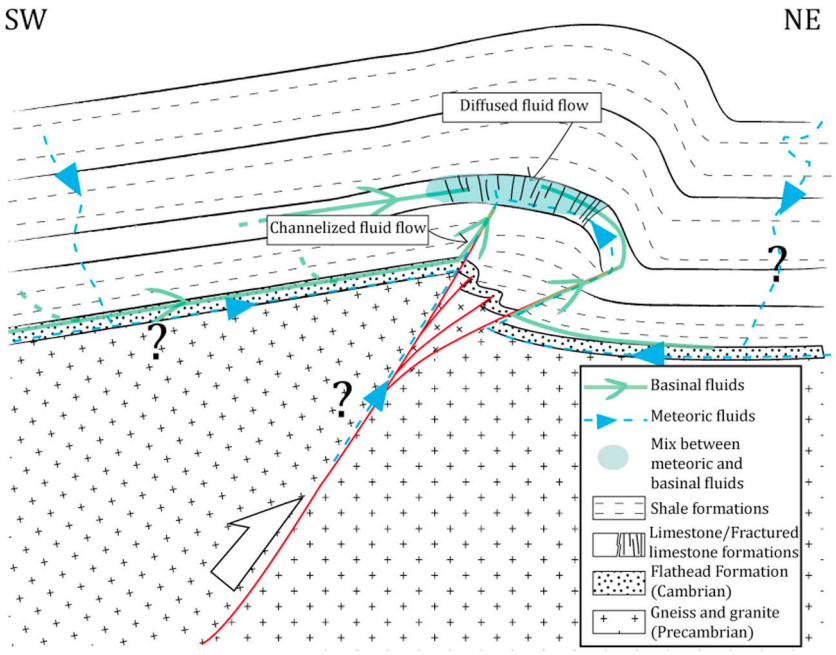

Figure 9. Conceptual model of fluid system at Sheep Mountain Anticline, composed by a mix between basinal fluids and Paleogene meteoric fluids migrating in the Flathead sandstones and interacting with basement. Fluid migration is channelized along the thrust in the sedimentary cover through shale formations until fluids reach the fractured limestone formations and then diffused through the whole fracture pattern at fold scale thanks to synfolding set III fractures that enhanced overall fracture connectivity. The subsurface geometry was drawn according to *Amrouch et al.* [2010a].

[22] The fields and trends in Figure 4a define three important fluid behaviors that we believe accurately describe the paleohydrologic system at Sheep Mountain Anticline. Veins with $\delta^{18}O > -11.5‰$ were precipitated from fluids that were well equilibrated with the host rocks and/or are unrelated to the Laramide fluid system. All other veins relate to the Laramide fluid system, and can be divided into two groups, depending on their degree of mixing and host rock interaction. We interpret that veins with isotopic signature close to Paleogene meteoric water ($\delta^{18}O < -19‰$) precipitated from rapidly migrating fluids that did not equilibrate with the host rocks and did not significantly mix with other formations or basinal waters. As this primarily concerns set III fractures, it suggests that these fractures were an efficient conduit for fluid flow. In the contrary, we interpret veins with a $\delta^{18}O$ values between −19‰ and −11.5‰ as reflecting slower fluid migration and consequently, varying degrees of fluid-rock interaction and mixing with basinal or formation waters. Most of set II veins are into this group, suggesting that this set was a poorly efficient conduit. Some veins from each set fall into these two fluid behaviors, suggesting that some early formed fractures were reopened and were hydraulically conductive at different times during fold growth, implying that in response to strata bending, some set I fractures were reopened [*Fiore Allwardt et al.*, 2007], while some set II veins were either reopened or newly formed during strata curvature [*Bergbauer and Pollard*, 2004]. Further evidence for chemical solution of some set II veins comes from our observations of multiple generations of filling and dissolution (Figure 3c).

[23] A possible scenario of fluid flow during Laramide contractional event can therefore be proposed. Paleogene meteoric fluids migrated downward and were heated up to reach at least 115°C. During LPS, heated meteoric fluids migrated upward in a poorly connected fracture pattern composed mainly by set I and set II fractures, where they were mixed with basinal fluids and cooled down. Cements precipitating from this fluid mix were partially equilibrated with host rocks. Later, synfolding strata bending enhanced connectivity of the different fracture sets by creating set III fractures and by reopening set I and II veins, allowing heated meteoric fluid to migrate upward rapidly with limited chemical and thermal interactions with country rocks (Figure 9).

5.3. Paleofluid Migration Pathways

[24] As suggested by isotope signatures of oxygen and carbon coupled with microthermometric data, the main fluid involved in the paleofluid system is a meteoric fluid heated to at least 115°C. Considering a geothermal basinal gradient of 30°C/km and a 3000 m thick sedimentary cover at SMA [*Hennier*, 1984], a meteoric fluid with a temperature of 10–15°C at the surface would reach this 115°C minimum temperature when flowing at a depth greater than the basement-cover interface, where the temperature was most probably only about 100°C. Given that the homogenization temperature of fluid inclusions is an estimate of the minimal temperature reached by the fluids at the time of precipitation, meteoric fluids necessarily migrated to a minimum depth of 1 km within the basement, where a Laramide geothermal gradient is about 20°C to 29°C/km [*Brigaud et al.*, 1990]. Radiogenic $^{87}Sr/^{86}Sr$ ratios suggest a more or less efficient mix of Paleogene meteoric fluids with basinal fluids (Figure 6). However, the most radiogenic samples could reflect little interactions with basement rocks, suggesting a short migration of fluids in the basement, as also suggested by *Katz et al.* [2006], before they mix with basinal fluids. Therefore, at the basin scale, there are two possible migration pathways for the meteoric fluid: (1) this fluid flowed from the west, through the 6 km thick sedimentary cover of the Bighorn Basin [*Stone*, 1993], in the Cambrian Flathead Formation, described as continuous sandstones with high permeability and a good potential reservoir [*Bell*, 1970], or (2) fluid migrated from the east, where the Bighorn Mountains elevation since the upper Cretaceous [*Crowley et al.*, 2002] provided the driving force required for downward fluid migration along basement faults. In such case, the flow must have occurred in the basement, as nowhere was the basement-cover interface deeper than 3 km.

5.4. Structural Implications

[25] To date, the geometry of the thrust underlying SMA is still debated. The Laramide fluid system defined here implies a fast upward migration of Paleogene meteoric fluids from the base of the sedimentary cover toward the studied formations, i.e., through 1000 m thick formations of nonpermeable shales [*Hennier*, 1984]. Thus, geochemical data support the interpretation that an efficient conduit, which could be the underlying thrust, was active during fold growth. This also is consistent with the published cross sections which make SMA a structure similar to the structure of Rattlesnake Mountain Anticline, a fold located on the western edge of the basin [e.g., *Stearns*, 1971; *Erslev*, 2005; *Neely and Erslev*, 2009]. Our geochemical data (Figure 5) demonstrate a structural control on the fluid migration in this basement-cored fold. This contrasts with décollement folds, wherein there is no structural control on the fluid migration at the fold scale [*Fischer et al.*, 2009], likely because there is no efficient conduit beneath the folded strata. Thus, in fault-related basement-cored folds, fluids most likely flow along the thrusts and, above their tips, flow through the diffuse fracture network of the sedimentary cover which is connected thanks to the curvature-related fractures.

[26] Geochemical data show that there is no difference in the paleofluid system in the rabbit ear structure and SMA (Figure 4). This rabbit ear structure was classically interpreted as a late structure related to a décollement in the shales of the Cambrian Gros Ventre formation [*Hennier and Spang*, 1983] and possibly connected to the Rio thrust [*Stanton and Erslev*, 2004]. As this rabbit ear structure strikes parallel to most of the Bighorn Basin Laramide folds, *Amrouch et al.* [2010a] proposed that this décollement level is connected to a preexisting basement fault. Because the isotopic pattern (Figure 4) shows that the fluid system involved in the hinge of the rabbit ear is consistent with that of SMA, one can safely propose that the growth of this secondary structure was probably synchronous with SMA growth.

6. Conclusions

[27] The combination of C, O and Sr isotopic data with microstructural observations and fluid inclusion microthermometry constrains the nature of the fluid system associated with development of the Laramide thrust-related, basement-cored Sheep Mountain Anticline. This fluid system is made of Paleogene meteoric fluid heated up at depth to a minimal temperature of 115°C and mixed in the cover with basinal fluids. During a first stage, heated meteoric fluids flowed slowly through reactivated prefolding fractures and in some newly formed layer parallel shortening-related fractures. During fold growth, while strata curvature created synfolding fractures with high vertical and lateral connectivity, heated fluids flowed and precipitated faster, without strong mixing with basinal fluids and equilibration with their host rocks.

[28] The geochemical signatures of calcite veins witness a fast upward migration of fluids through impermeable shales, requiring the existence of a fault in the sedimentary cover. Our study suggests that, in thick-skinned forelands, fluids flow along basement thrusts, and, above their tip, in secondary faults and diffuse fractures. It also illustrates the feasibility and the interest of a coupled geochemical and microstructural study of paleofluids from cements of diffuse fractures.

Acknowledgments

[29] The authors acknowledge the help of M. de Rafélis for cathodoluminescence analyses and of J. Thibieroz for providing the microthermometric stage and for his advice for the fluid inclusion study. We also thank N. Labourdette from the Biominéralisation et Environnements Sédimentaires team of ISTEP for her involvement in the isotopic analyses. We thank the *G-Cubed* Editor Louis Derry and the reviewers Mark P. Fischer and Brian Stewart for their revisions and helpful comments, which have greatly improved the earlier version of the manuscript.

References

Amrouch, K., O. Lacombe, N. Bellahsen, J. M. Daniel, and J. P. Callot (2010a), Stress and strain patterns, kinematics and deformation mechanisms in a basement-cored anticline: Sheep Mountain Anticline, Wyoming, *Tectonics*, *29*, TC1005, doi:10.1029/2009TC002525.

Amrouch, K., P. Robion, J. P. Callot, O. Lacombe, J. M. Daniel, N. Bellahsen, and J. L. Faure (2010b), Constraints on deformation mechanisms during folding provided by rock physical properties: A case study at Sheep Mountain anticline (Wyoming, USA), *Geophys. J. Int.*, *182*, 1105–1123, doi:10.1111/j.1365-246X.2010.04673.x.

Bell, L. H. (1970), Depositional history of the Cambrian Flathead Standstone, Park County, Wyoming, *Wyo. Geol. Assoc. Guideb.*, *22*, 115–131.

Bellahsen, N., P. Fiore, and D. D. Pollard (2006a), The role of fractures in the structural interpretation of Sheep Mountain Anticline, Wyoming, *J. Struct. Geol.*, *28*(5), 850–867, doi:10.1016/j.jsg.2006.01.013.

Bellahsen, N., P. Fiore, and D. D. Pollard (2006b), From spatial variation of fracture patterns to fold kinematics: A geomechanical approach, *Geophys. Res. Lett.*, *33*, L02301, doi:10.1029/2005GL024189.

Bergbauer, S., and D. Pollard (2004), A new conceptual fold-fracture model including prefolding joints, based on the Emigrant Gap anticline, Wyoming, *Geol. Soc. Am. Bull.*, *116*(3), 294–307, doi:10.1130/B25225.1.

Bjorøy, M., J. Williams, D. Dolcater, M. Kemp, and J. Winters (1996), Maturity assessment and characterization of Big Horn Basin Palaeozoic oils, *Mar. Pet. Geol.*, *13*(1), 3–23, doi:10.1016/0264-8172(95)00018-6.

Bodnar, R. J. (2003), Introduction to fluid inclusions, in *Fluid Inclusions: Analysis and Interpretation*, edited by I. Samson, A. Anderson, and D. Marshall, *Short Course Ser. Mineral. Assoc. Can.*, *32*, 1–8.

Boles, J. R., P. Eichhubl, G. Garven, and J. Chen (2004), Evolution of a hydrocarbon migration pathway along basin-bounding faults: Evidence from fault cement, *AAPG Bull.*, *88*(7), 947–970, doi:10.1306/02090403040.

Bottinga, Y. (1969), Calculated fractionation factors for carbon and hydrogen isotope exchange in the system calcite-carbon dioxide-graphite-methane-hydrogen-water vapor, *Geochim. Cosmochim. Acta*, *33*, 49–64, doi:10.1016/0016-7037(69)90092-1.

Brigaud, F., D. S. Chapman, and S. Le Douaran (1990), Estimating thermal conductivity in sedimentary basins using lithologic data and geophysical well logs, *AAPG Bull.*, *74*(9), 1459–1477.

Bruckschen, P., S. Oesmann, and J. Veizer (1999), Isotope stratigraphy of the European Carboniferous: Proxy signals for ocean chemistry, climate and tectonics, *Chem. Geol.*, *161*, 127–163, doi:10.1016/S0009-2541(99)00084-4.

Bussolotto, M., A. Benedicto, C. Invernizzi, L. Micarelli, V. Plagnes, and G. Deina (2007), Deformation features within an active normal fault zone in carbonate rocks: The Gubbio fault (Central Apennines, Italy), *J. Struct. Geol.*, *29*, 2017–2037, doi:10.1016/j.jsg.2007.07.014.

Cazenave, S., R. Chapoulie, and G. Villeneuve (2003), Cathodoluminescence of synthetic and natural calcite: The effects of manganese and iron on orange emission, *Mineral. Petrol.*, *78*(3–4), 243–253, doi:10.1007/s00710-002-0227-y.

Chapoulie, R., S. Cazenave, and A. Cerepi (2005), Apport de la cathodoluminescence à haute résolution à l'étude de la diagenèse météorique dans les formations sédimentaires carbonatées, *C. R. Geosci.*, *337*(3), 337–346, doi:10.1016/j.crte.2004.10.008.

Chung, H., S. Brand, and P. Grizzle (1981), Carbon isotope geochemistry of Paleozoic oils from Big Horn Basin, *Geochim. Cosmochim. Acta*, *45*, 1803–1815, doi:10.1016/0016-7037(81)90011-9.

Conti, A., L. Turpin, R. Polino, M. Mattei, and G. M. Zuppi (2001), The relationship between evolution of fluid chemistry and the style of brittle deformation: Examples from the Northern Apennines (Italy), *Tectonophysics*, *330*, 103–117, doi:10.1016/S0040-1951(00)00224-9.

Crowley, P. D., P. W. Reiners, J. M. Reuter, and G. D. Kaye (2002), Laramide exhumation of the Bighorn Mountains, Wyoming: An apatite (U-Th)/He thermochronology study, *Geology*, *30*(1), 27–30, doi:10.1130/0091-7613(2002)030<0027:LEOTBM>2.0.CO;2.

Dietrich, D., J. A. McKenzie, and H. Song (1983), Origine of calcite in syntectonic veins as determined from carbon-isotopes ratios, *Geology*, *11*, 547–551, doi:10.1130/0091-7613(1983)11<547:OOCISV>2.0.CO;2.

Donovan, T. J., I. Friedman, and J. D. Gleason (1974), Recognition of petroleum-bearing traps by unusual isotopic compositions of carbonate-cemented surface rocks, *Geology*, *2*, 351–354, doi:10.1130/0091-7613(1974)2<351:ROPTBU>2.0.CO;2.

Douglas, T., C. Chamberlain, M. Poage, M. Abruzzese, S. Shultz, J. Henneberry, and P. Layer (2003), Fluid flow and the Heart Mountain fault: A stable isotopic, fluid inclusion and geochronologic study, *Geofluids*, *3*, 13–32, doi:10.1046/j.1468-8123.2003.00049.x.

Erslev, E. A. (2005), 2D Laramide geometries and kinematics of the Rocky Mountains, *The Rocky Mountain Region: An Evolving Lithosphere Tectonics, Geochemistry, and*

Geophysics, *Geophys. Monogr. Ser.*, vol. 154, edited by K. E. Karlstrom and G. R. Keller, pp. 7–20, AGU, Washington, D. C.

Evans, M. A., and G. C. Hobbs (2003), Fate of 'warm' migrating fluids in the central Appalachians during the Late Paleozoic Alleghanian orogeny, *J. Geochem. Explor.*, *78–79*, 327–331, doi:10.1016/S0375-6742(03)00088-8.

Faure, G., and J. L. Powell (1972), *Strontium Isotope Geology*, 166 pp., Springer, New York.

Fiore Allwardt, P., N. Bellahsen, and D. D. Pollard (2007), Curvature and fracturing based on global positioning system data collected at Sheep Mountain Anticline, Wyoming, *Geosphere*, *3*(6), 408–421, doi:10.1130/GES00088.1.

Fischer, M. P., I. Camilo Higuera-Díaz, M. A. Evans, E. C. Perry, and L. Lefticariu (2009), Fracture-controlled paleohydrology in a map-scale detachment fold: Insights from the analysis of fluid inclusions in calcite and quartz veins, *J. Struct. Geol.*, *31*, 1490–1510.

Foreman, J. L., and W. M. Dunne (1991), Condition of vein formation in the southern Appalachian foreland: Constraints from vein geometries and fluid inclusions, *J. Struct. Geol.*, *13*(10), 1173–1183, doi:10.1016/0191-8141(91)90076-U.

Forster, A., A. P. Irmen, and C. Vondra (1996), Structural interpretation of Sheep Mountain Anticline, Bighorn Basin, Wyoming, *Wyo. Geol. Assoc. Guideb.*, *47*, 239–251.

Goldstein, R. H., and T. J. Reynolds (1994), *Systematics of Fluid Inclusions in Diagenetic Minerals*, *SEPM Short Course*, *31*, 199 pp.

Hanor, J. S. (1980), Dissolved methane in sedimentary brines: Potential effect on the PVT properties of fluid inclusions, *Econ. Geol.*, *75*, 603–609, doi:10.2113/gsecongeo.75.4.603.

Harris, J. F., G. L. Taylor, and J. L. Walper (1960), Relation of deformational fractures in sedimentary rocks to regional and local structures, *AAPG Bull.*, *44*, 1853–1873.

Hathaway, J. C., and E. G. Degens (1969), Methane-derived marine carbonates of Pleistocene age, *Science*, *165*(3894), 690–692, doi:10.1126/science.165.3894.690.

Hennier, J. H. (1984), Structural analysis of the Sheep Mountain Anticline, Bighorn Basin, Wyoming, M.S. thesis, 118 pp., Tex. A&M Univ., College Station.

Hennier, J., and J. H. Spang (1983), Mechanisms for deformation of sedimentary strata at Sheep Mountain anticline, Bighorn basin, Wyoming, *Wyo. Geol. Assoc. Guideb.*, *34*, 96–111.

Johnson, G. D., L. J. Garside, and A. J. Warner (1965), A study of the structure and associated features of Sheep Mountain Anticline, Big Horn County, Wyoming, *J. Iowa Acad. Sci.*, *72*, 332–342.

Katz, D. A., G. P. Eberli, P. K. Swart, and L. B. Smith Jr. (2006), Tectonic-hydrothermal brecciation associated with calcite precipitation and permeability destruction in Mississippian carbonate reservoirs, Montana and Wyoming, *AAPG Bull.*, *90*, 1803–1841, doi:10.1306/03200605072.

Kim, S.-T., and J. R. O'Neil (1997), Equilibrium and nonequilibrium oxygen isotope effects in synthetic carbonates, *Geochim. Cosmochim. Acta*, *61*(16), 3461–3475, doi:10.1016/S0016-7037(97)00169-5.

Koch, P. L., J. C. Zachos, and D. L. Dettman (1995), Stable isotope and paleoclimatology of the Paleogene Bighorn Basin (Wyoming, USA), *Palaeogeogr. Palaeoclimatol. Palaeoecol.*, *115*, 61–89, doi:10.1016/0031-0182(94)00107-J.

Lefticariu, L., E. C. Perry, M. P. Fischer, and J. L. Banner (2005), Evolution of fluid compartmentalization in a detachment fold complex, *Geology*, *33*(1), 69–72, doi:10.1130/G20592.1.

Marquer, D., and M. Burkhard (1992), Fluid circulation, progressive deformation and mass-transfer processes in the upper crust: The example of basement-cover relationships in the External Crystalline Massifs, Switzerland, *J. Struct. Geol.*, *14*(8–9), 1047–1057, doi:10.1016/0191-8141(92)90035-U.

Neely, T., and E. Erslev (2009), The interplay of fold mechanisms and basement weaknesses at the transition between Laramide basement-involved arches, north-central Wyoming, USA, *J. Struct. Geol.*, *31*, 1012–1027, doi:10.1016/j.jsg.2009.03.008.

Ramsey, D. W., and C. M. Onasch (1999), Fluid migration in a cratonic setting: The fluid histories of two fault zones in the eastern midcontinent, *Tectonophysics*, *305*, 307–323, doi:10.1016/S0040-1951(99)00021-9.

Rhodes, M. K., A. R. Carroll, J. T. Pietras, B. L. Beard, and C. M. Johnson (2002), Strontium isotope record of paleohydrology and continental weathering, Eocene Green River Formation, Wyoming, *Geology*, *30*(2), 167–170, doi:10.1130/0091-7613(2002)030<0167:SIROPA>2.0.CO;2.

Rosenbaum, J., and S. M. F. Sheppard (1986), An isotopic study of siderites, dolomites and ankerites at high temperatures, *Geochim. Cosmochim. Acta*, *50*(6), 1147–1150, doi:10.1016/0016-7037(86)90396-0.

Roure, F., R. Swennen, F. Schneider, J. L. Faure, H. Ferkand, N. Guilhaumou, K. Osadandz, P. Robion, and V. Vandeginste (2005), Incidence and importance of tectonics and natural fluid migration on reservoir evolution in foreland fold-and-thrust belts, *Oil Gas Sci. Technol.*, *60*(1), 67–106, doi:10.2516/ogst:2005006.

Savage, H. M., J. R. Shackleton, M. L. Cooke, and J. J. Riedel (2010), Insights into fold growth using fold-related joint patterns and mechanical stratigraphy, *J. Struct. Geol.*, *32*, 1466–1475, doi:10.1016/j.jsg.2010.09.004.

Stanton, H. I., and E. A. Erslev (2004), Sheep Mountain Anticline: Backlimb tightening and sequential deformation in the Bighorn Basin, Wyoming., *Wyo. Geol. Assoc. Guideb.*, *53*, 75–87.

Stearns, D. W. (1971), Mechanisms of drape folding in the Wyoming Province, *Wyo. Geol. Assoc. Guideb.*, *23*, 125–144.

Stone, D. S. (1967), Theory of Paleozoic oil and gas accumulation in Bighorn Basin, Wyoming, *Am. Assoc. Pet. Geol. Bull.*, *51*, 2056–2114.

Stone, D. S. (1993), Basement-involved thrust-generated folds as seismically imaged in the subsurface of the central Rocky Mountain foreland, in *Laramide Basement Deformation in the Rocky Mountain Foreland of the Western United States*, edited by C. J. Schmidt, R. B. Chase, and E. A. Erslev, *Spec. Pap. Geol. Soc. Am.*, *280*, 271–318.

Stone, D. S. (2004), Rio thrusting, multi-stage migration and formation of vertically segregated Paleozoic oil pools at Torchlight Field on the Greybull Platform (Eastern Bighorn basin): Implication for exploration, *Mt. Geol.*, *41*, 119–138.

Templeton, A. S., J. Sweeney Jr., H. Manske, J. F. Tilghman, S. C. Calhoun, A. Voilich, and C. P. Chamberlain (1995), Fluids and the Heart Mountain fault revisited, *Geology*, *23*(10), 929–932, doi:10.1130/0091-7613(1995)023<0929:FATHMF>2.3.CO;2.

Travé, A., F. Calvet, M. Sans, J. Vergés, and M. Thirlwall (2000), Fluid history related to the Alpine compression at the margin of south-Pyrenean Foreland basin: The El Guix anticline, *Tectonophysics*, *321*, 73–102, doi:10.1016/S0040-1951(00)00090-1.

Travé, A., P. Labaume, and J. Vergés (2007), Fluid Systems in foreland fold-and-thrust belts: An overview from the Southern Pyrenees, in *Thrust Belts and Foreland Basins*, edited by O. Lacombe, J. Lavé, F. Roure, and J. Vergés, pp. 93–115, Springer, Berlin, doi:10.1007/978-3-540-69426-7_5.

Van Geet, M., R. Swennen, C. Durmishi, F. Roure, and P. Muchez (2002), Paragenesis of Cretaceous to Eocene carbonate reservoirs in the Ionian fold and thrust belt (Albania): Relation between tectonism and fluid flow, *Sedimentology*, *49*, 697–718, doi:10.1046/j.1365-3091.2002.00476.x.

Zheng, Y. F. (1999), Oxygen isotope fractionation in carbonate and sulphate minerals, *Geochem. J.*, *33*, 109–126.